A novel torsion/bending element for Dynamic Relaxation Modeling

Authors:

Michael R BARNES[a], Sigrid ADRIAENSSENS[b], Meghan KRUPKA[b]

[a] Emeritus Professor of Department of Architecture and Civil Engineering,

University of Bath, Bath, BA2 7AY, United Kingdom

[b]Department of Civil and Environmental Engineering,

Princeton University, Princeton, 08544, NJ, United States of America

E-mail: sadriaen@princeton.edu

Tel: ++ 1 609 258 4661

Fax: ++ 1609 258 2760

Corresponding author: Sigrid ADRIAENSSENS

Abstract

This paper proposes and validates a three degrees of freedom element formulation that accounts for torsion and transverse bending of three-dimensional curved elements in explicit numerical analyses methods such as Dynamic Relaxation. Using finite difference modeling, in-plane distortions and moments, the increment of twist (and hence torsion) and out-of-plane bending deformations are determined. Numerical stability and convergence limits of the element are discussed. Two sets of circular arc test cases validate the accuracy of the element against theoretical and six degrees of freedom finite-element results. This element is widely applicable and found in strained grid shells and spline stressed membranes.

Keywords: form-finding, structural analysis, finite difference, dynamic relaxation, bending, torsion

1. Introduction

Early tensile structures, though elegant in shape, were crude in detail as a result of the technology that was still under development, and also due to a lack of awareness of the importance of the shaping and supporting elements in the new architecture that was being generated. Systems that shape technical textiles must be expressive of their function and the materials that they are made of. Ultimately, these systems which can include compression masts, ring beams and spatially curved systems must be as refined as the fabric itself. The aesthetics created by the slenderness and delicate equilibrium between compression, tension and curved elements in systems such as a model for a crane [1] and the more recent design for a solar shade [2] (see Figure 1a and b) have been a point of reference for this paper. The physical crane model consists of a central flexible tapering continuous steel member, plexi glass three pointed stars of diminishing size equi-spaced on the central member, and three sets of nylon cables. A nylon cable is attached to the end of each star and runs through holes in the underlying stars to a control

mechanism at the foot of the crane. Spatial curves such as three-dimensional S-shapes are achieved by applying different tension forces to individual cables within one series. The more recent model for a solar shade design consists of three cantilevering structural spatially curved units. Each unit relies on a flexible yet strong three-dimensional boundary curved element, twisted and bent into shape by the pre-stress in the attached flexible membrane.

A desirable aspect in explicit numerical form-finding and load analysis (such as Dynamic Relaxation DR) for such bending/torsion element-membrane systems (see Figure 1b) is the treatment of the curved element as a finite difference continuum. Current element formulations that have been developed for DR to enable form finding and load analysis of non-linear structures are not focused on modeling the torsion/bending action. Day [3] derived the concept of Dynamic Relaxation as an explicit solution method for the static behavior of structures from an analogy with tidal flow computations. Equations of damped structural motion and the constitutive equations of elasticity substituted respectively for the equations of fluid motion and continuity. Brew and Brotton [4] developed a DR formulation that separated the equations for equilibrium and compatibility (motion) and did not require the formulation of the overall stiffness matrix. This vector form of DR has become the most widely used, particularly for highly non-linear structures, and is adopted in this paper with a kinetic damping approach [5]. This numerical method has been extensively researched and improved in the works of Barnes [6], Papadrakakis [7], Wakefield [8], Topping [9] (and more recently Wood [10] and Hand and Lee [11]). For a comprehensive description of the DR method the reader is referred to Topping [12]. Besides improving the numerical method, Barnes developed and validated formulations for specific element types such as strut and cable links and membrane elements that account for cable slackening, membrane buckling and non-linear material properties. To enable the form-finding and analysis of a wide range of structures, more recent element developments have included alternative membrane (Gosling and Lewis [13], Hegyi et al. [14]) and pneumatic elements (Rodriguez et al. [15]), non regular tensegrity modules (Zhang et al. [16]) (Bel Hadj. Ali et al. [17]), reciprocal frames links (Douthe and Baverel [18]),pulley elements with friction (Hincz

[19]) and beam elements (Adriaenssens and Barnes [20]). The novel bending/torsion element presented in this paper has significant advantages in a DR scheme since it requires only three translational degrees of freedom per node. Rotational degrees of freedom are not required, and it is often the coupling of these with axial stiffness and translational degrees of freedom that can cause conditioning problems in explicit numerical methods.

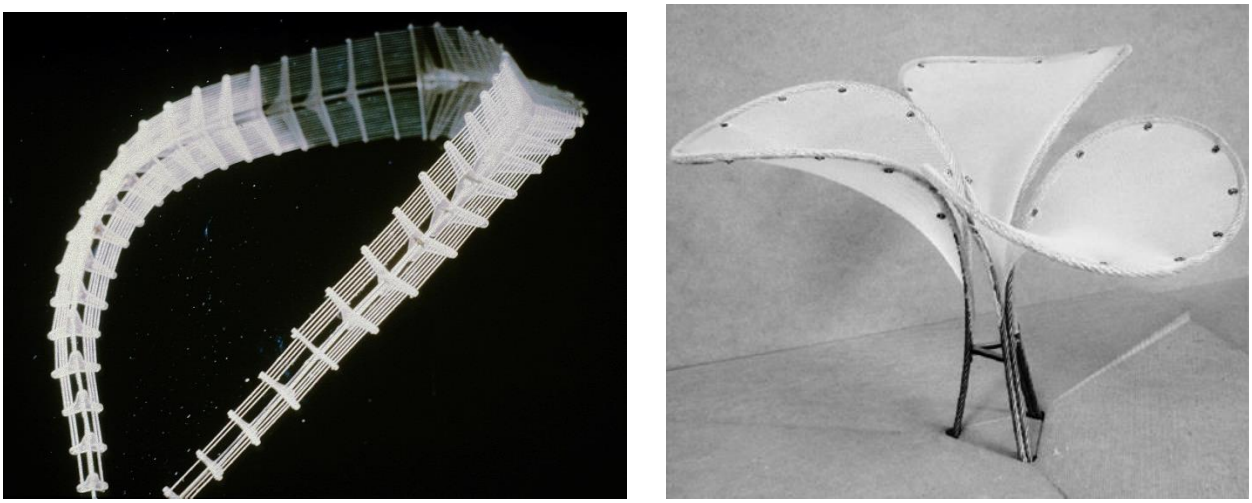

Figure 1 (a): crane model, a central flexible curve element is shaped by three sets of longitudinal cables (photo courtesy ILEK,Institut für Leichtbau Entwerfen und Konstruieren) **(b)** a twisted and bent element equilibrates with a pre-stressed membrane to form a sun shading structure.(Princeton University student project photo courtesy S Bagrianski, A Heid and M Krupka)

2. Method

2.1. Dynamic Relaxation Scheme

The basis of the dynamic relaxation method adopted in this paper is to trace step-by-step for small time increments, Δt , the motion of each node of a structure until, due to artificial damping, the structure comes to rest in static equilibrium. In form-finding the process may be started from an arbitrary specification of geometry, with the motion caused by imposing a stress or force specification in some or all of the

structure components. The form-finding is usually carried out for a weightless state since, after obtaining an equilibrium state, this allows a subsequent factoring of the pre-stress forces in all components without affecting the geometry. For load analyses, which must start from the pre-stress equilibrium state, the motion is caused by suddenly applying the loading. The description of DR summarized briefly below for skeletal structures with strut and cable links assumes "kinetic" damping of the structural system to obtain a static equilibrium state [21]. In this procedure the undamped motion of the structure is traced and when a local peak in the total kinetic energy of the system is detected, all velocity components are set to zero. The process is then restarted from the current geometry and repeated through further (generally decreasing) peaks until the energy of all modes of vibration have been dissipated and static equilibrium is achieved. The dynamic relaxation formulation uses Newton's second law governing the motion of any node i in direction *x* at time *t*:

$$R_{ix}^{t} = M_i \dot{v}_{ix}^{t} \tag{1}$$

Where

R_{ix}^{t} residual force at node *i* in direction *x* at time *t*, M_i lumped mass at node *i* , set to optimize convergence and ensure stability of the numerical process [6], $\dot{v}_{ix}^{t}$ acceleration at node *i* in direction *x* at time *t*

Expressing the acceleration term in Eq. (1) in finite difference form and rearranging the equation gives the recurrence equation for updating the velocity components:

$$v_{ix}^{t+\Delta t/2} = \frac{\Delta t}{M_i} R_{ix}^{t} + v_{ix}^{t-\Delta t/2} \tag{2}$$

Hence the updated geometry projected to time $t + \Delta t/2$

$$x_i^{t+\Delta t} = x_i^t + \Delta t v_{ix}^{t+\Delta t/2}$$

(3)

Eqs. (2) and (3) apply for all unconstrained nodes of the mesh in each coordinate direction. These equations are nodally decoupled in the sense that the updated velocity components are dependent only on previous velocity and residual force components at a node. They are not directly influenced by the current $t + \Delta t/2$ updates at other nodes. Having obtained the complete updated geometry the new link forces can be determined and resolved together with any the applied load components P_{ix} to give the updated residuals:

$$R_{ix}^{t+\Delta t} = P_{ix} + \sum (\frac{F}{L})_m^{t+\Delta t} (x_j - x_i)^{t+\Delta t}$$

(4)

for all elements *m* connecting to *i*,

Where $F_m^{t+\Delta t}$ force in member *m* connecting node *i* to an adjacent node *j* at time $t + \Delta t$, $L_m^{t+\Delta t}$ length of member *m* at time $t + \Delta t$, calculated using Pythagoras's theorem in three dimensions.

The procedure is thus time stepped using Eqs. (2)–(4) until a kinetic energy peak is detected. Velocity components are then reset to zero (with a small adjustment made to the geometry to correct to the true kinetic energy time peak), and the process is repeated until adequate convergence is achieved.

2.2. Existing In-Plane Bending Element Formulation

To deal with moments and shear forces when initially straight tubular members are deformed (such as the central core in figure 1a), a spline type formulation can be used as proposed by Adriaenssens and Barnes [20]. The scheme adopts a finite difference modeling of a continuous beam. Figure 2a represents consecutive nodes along an initially straight tubular beam traverse, and Figure 2b two adjacent deformed

segments, a and b, viewed normal to the plane of nodes ijk which are assumed to lie on a circular arc of radius *R*. The spacing of nodes along the traverse must be sufficiently close to model this, but the segment lengths need not be equal. The radius of curvature *R* through ijk and the bending moment *M* in the arc can be defined as

$$R = \frac{l_c}{2\sin\alpha} \text{ and } M = \frac{EI}{R} \tag{5}$$

Where *EI* is assumed to be constant along the beam, *E* is modulus of elasticity and *I* second moment of area. The free body shear forces S_a, S_b of elements *a* an *b* complying with moment *M* at *j* are thus:

$$S_a = \frac{2EI\sin\alpha}{l_a.l_c} \text{ and } S_b = \frac{2EI\sin\alpha}{l_b.l_c} \tag{6}$$

Where l_a, l_b, l_c are the distances between nodes *ij, jk* and *ik* respectively. The three non-collinear nodes *i,j* and *k* define a two-dimensional surface, referred to in this paper as the plane *ijk*.
These shear forces S_a and S_b are applied at nodes *i,j* and *j,k* respectively and act normal to the links *ij* and *jk* respectively within the plane *ijk.* The shear forces act in the direction of the bending moment *M* at the middle node *j* and in the opposite direction at nodes *i* and *k*. . The calculations and transformations required in DR scheme are thus rather simple, with sets of three consecutive nodes being considered sequentially along the entire transverse, each lying in different planes when modeling a spatially curved tube bent from an initially straight condition. The formulation is useful for modeling grid shells employing continuous tubular members, and also for membranes in which flexible battens are employed to give shape control (as in some sails). The technique can also be extended to deal approximately with plane circular arcs (either initially strained or unstrained). To deal with the more general case of initially unstrained and spatially curved tubular members (such as the one depicted in figure 1b) it is necessary to account additionally for both torsion and transverse (out-of-plane) bending effects.

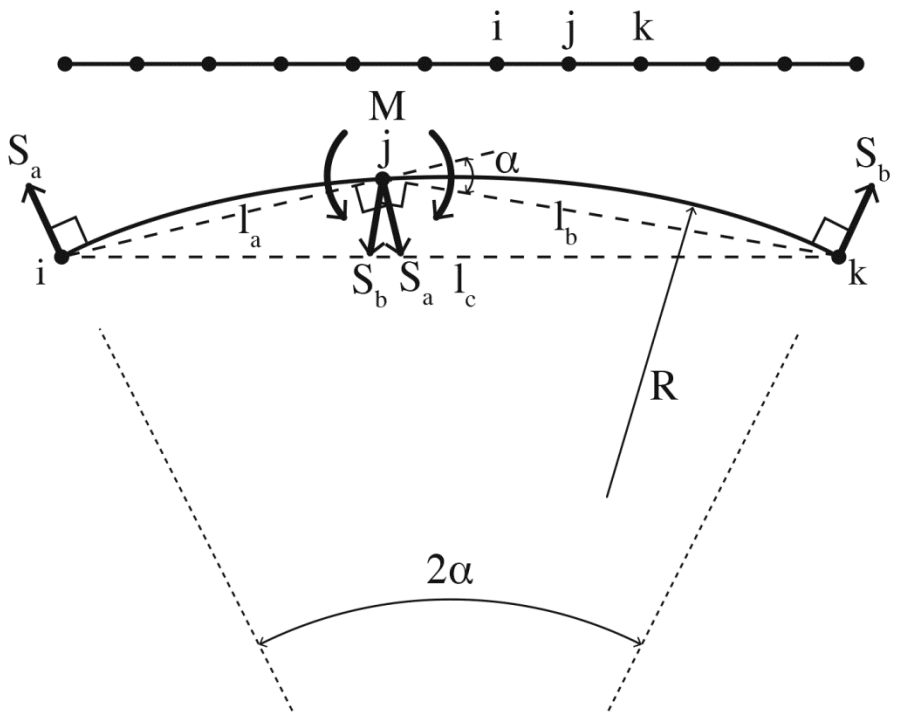

Figure 2: (a) Consecutive nodes along an initially straight tubular beam traverse; (b) Two adjacent deformed segments, a and b, viewed normal to the plane *ijk*.

2.3. Novel Torsion and Transverse Bending Element Formulation

2.3.1. Theory

For initially unstrained spatially curved arcs the local in plane bending can be dealt with in a similar way as presented in section 2.2,but with the local moments set as $M = EI\left(1/R - 1/R_0\right)$ where R_0 is the original radius of curvature and the shear forces (equivalent to equation 6) revised accordingly. The following theory accounts also for torsion and transverse bending moments in such spatial arc traverses. In most practical design cases, both deformations (transverse and radial deflections) and moments (torsional, transverse and radial bending) may be correctly modeled. This is achieved by applying an artificial "torsional factor" (which is the factor by which the real torsional stiffness *GJ* must be reduced in

order that transverse deformations may be correctly modeled. *G* is shear modulus of elasticity and *J* is the second polar moment of area). In some other more restrictive cases, for example with arch systems with a very low span to rise ratio (<150) and/or slenderness ratios which are very high (>500), the transverse deformations will be incorrectly modeled; however, even in these cases, an important feature which is still retained is that the transverse bending, radial, and torsional moments can be statically correctly modeled.

With only three translational degrees of freedom it is possible to determine by finite difference modeling the in-plane distortions and moments and the increment of twist and hence torsion in each link element of a spatially curved traverse, but it is not possible to determine directly also the transverse bending moments from deformations. However, assuming that the lines of action of all forces exerted by connecting elements (such as cables or membranes) act through the centerline of the curved element (i.e. with no applied torsion forces due to eccentricity of connections), the transverse moments are always statically related to the rate of change of torsions in the spatially curved element. For a small element of the curved element viewed normal to its local plane shown in Figure 3, the equilibrium of moments along axis t-t can be resolved as:

$$T + \frac{dT}{d\alpha}.d\alpha = M.\sin(d\alpha) + T.\cos(d\alpha) \tag{7}$$

and if $\alpha \to 0$ then $M = \frac{dT}{d\alpha}$ (8)

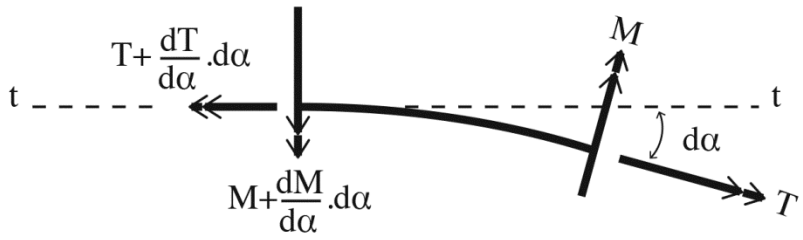

Figure 3: Free body diagram for a small element of a curved member.

Thus if the torsion in consecutive links and the local (in-plane) curvature is known the transverse (or out-of-plane) moment at the interconnecting node can be determined from equation 8. The in-plane moment was determined using two consecutive links. The initial amount of twist ϕ_i in any link and hence the torsion can be determined by considering three consecutive links going through the nodes i,j,k and m as shown in figure 4a and b. More specifically ϕ_i can be determined from the surface normal V_k and V_l at the nodes *k* and *l* of the oriented surfaces, defined by the nodes *i,k,l* and *k,l,m* respectively using the right-hand rule. If the shape of the element then changes (from figure 4b to figure 4c) and the resulting angle of twist $\phi' > \phi_i$, restoring forces P_m and P_j act at nodes *m* and *j* as well as associated forces P_k and P_l at nodes *k* and *l* due to torsion in link *kl*. P_m acts normal to the oriented surface defined by *k,l,m* and P_j acts in the opposite direction to the normal of the oriented surface defined by *j,k,l* result P_k acts normal to the oriented surface defined by *j,k,l* and P_j acts in the opposite direction to the normal of the oriented surface defined by *k,l,m*. These associated forces must act to restore the lateral moment equilibrium. P_j and P_m are related to the torsion *T* in link *kl* with link length L_{kl} *:*

$$P_j.h_j = P_m.h_m = T = \frac{GJ\left(\phi' - \phi_i\right)}{L_{kl}} \tag{9}$$

Where h_j and h_m are the heights of the triangles *jkl* and *klm* from the base *kl*.

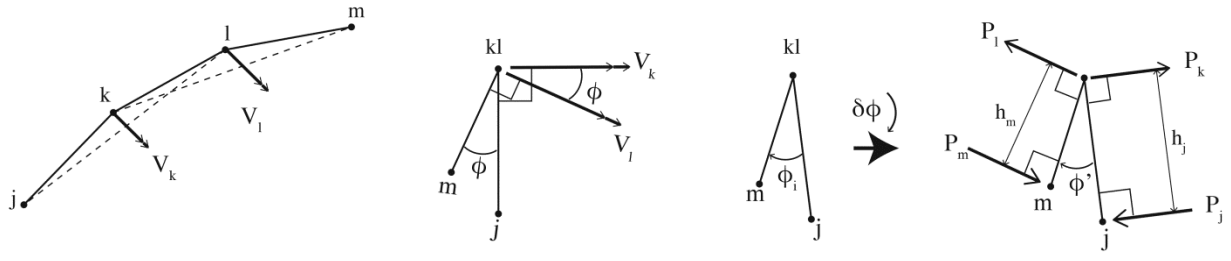

Figure 4 : (a) three consecutive links modeling a curved element going through nodes *j,k,l* and *m* and their normal vectors V_k and V_l at the nodes *k* and *l* of the oriented surfaces, determined by the right-hand rule and defined by the nodes *i,k,l* and *k,l,m* respectively (side view), **(b,c)** the current twist angle between them ϕ or the initial unstressed state of twist ϕ_i (view in direction parallel with kl), a change in the angle of twist $\delta\phi$ results in a new position **(d)** of the nodes j,k,l and m and sets up restoring forces P_m and P_j at nodes *m* and *j* due to torsion in link *kl* result as well as associated forces P_k and P_l at nodes *k* and *l* to restore the lateral moment equilibrium.

The axis zz, goes acts node *k* and lies in the bisector plane of the two planes defined by nodes *i.k,l* and *k,l,m*.

Considering static equilibrium of the 3 link configuration (shown in Figure 5) and resolving normal to the plane containing axis *zz,* and *kl*:

$$P_m \cos\left(\frac{\phi'}{2}\right) + P_k \cos\left(\frac{\phi'}{2}\right) = P_l \cos\left(\frac{\phi'}{2}\right) + P_j \cos\left(\frac{\phi'}{2}\right) \Leftrightarrow P_m + P_k = P_l + P_j \tag{10}$$

Taking moments about zz gives:

$$P_j.a + P_m.(b+c) = P_l.b \tag{11}$$

Where a,b and c are defined in Figure 5. Hence P_m and P_j can be determined from equation (9), and from (10) and (11) as:

$$P_l = \frac{\left(P_j.a + P_m.(b+c)\right)}{b} \text{ and } P_k = P_l + P_j - P_m \tag{12}$$

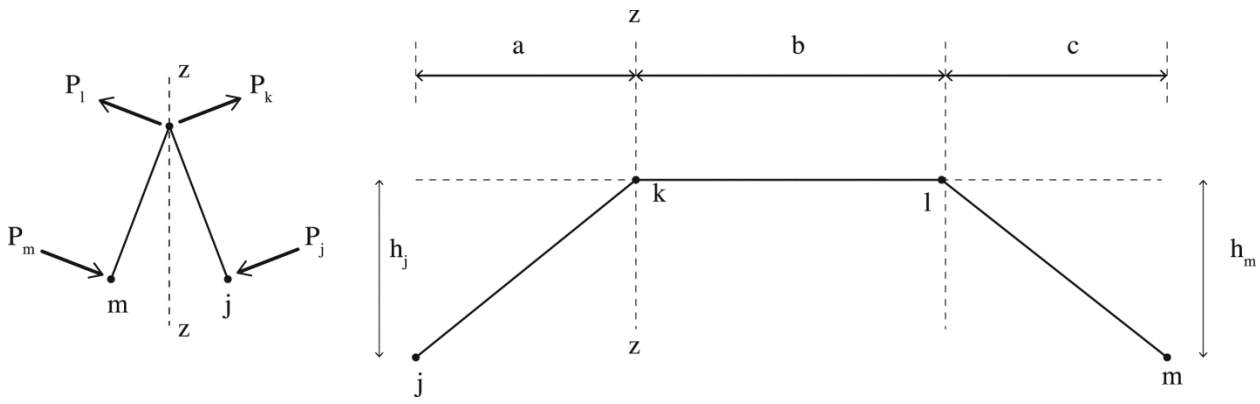

Figure 5: Static equilibrium of the three link unit and side view with dimensions.

In the situation of a shallow arc (assuming a consecutive links of similar lengths) the forces P_k and P_l are typically three times the values of P_m and P_j --those latter forces are determined directly in the DR process from current deformations. However the bending forces exerted by successive sets of three links along a curved element will tend to oppose and cancel each other, and will do so exactly if the torsions are constant (equation 8).

For curved elements with inflected sections (as shown in Figure 6), the expressions for P_m and P_j are given by equation 9, but the associated bending equilibrium forces are:

$$P_l = (P_m.(b+c) - P_j.a)/b \text{ and } P_k = P_m + P_j - P_l \tag{13}$$

In this paper the following sign convention is adhered to: for all cases provided $\delta\phi = \phi' - \phi_i$ is +ve (clockwise), P_j acts in the $-V_k$ direction and opposing P_k, and P_m acts in the $+V_l$ direction and opposing P_l.

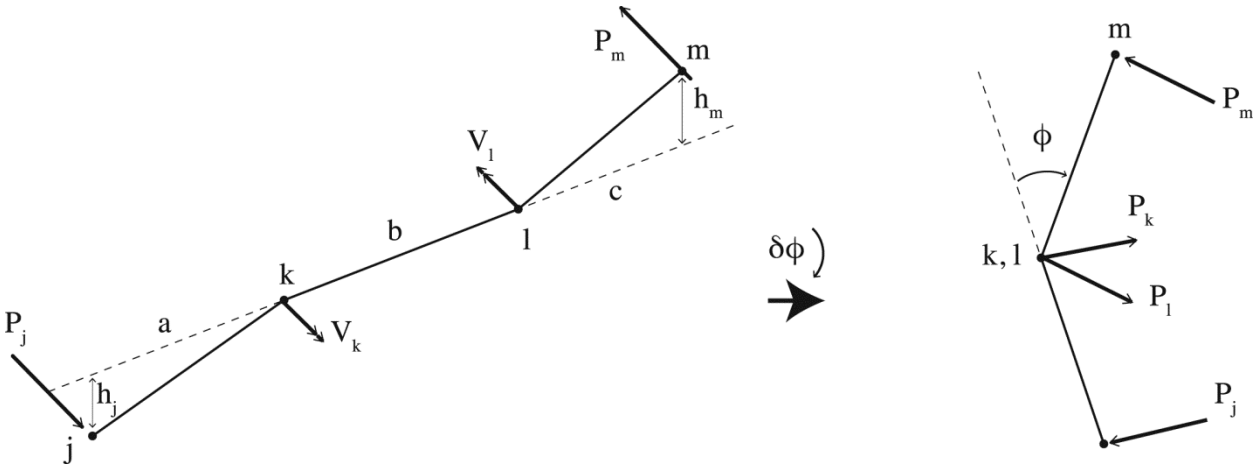

Figure 6: Forces acting on a curved element with inflected sections (**(a)** perspective and **(b)** view parallel with *kl*)

2.3.2. Torsion Factor

During the DR analysis the value of *GJ* in equation 9 governs the torsional deformations and hence also the associated transverse bending. In general, for open curved elements the torsional factor may vary quite widely depending particularly on the radius of curvature of the arch and the total arc length, but also being limited by the slenderness ratio and the span to rise ratio. Values for torsional factor in the case of open arches might be assessed by considering a circular arc beam with equal and opposite transverse loads applied at the quarter points, as shown in Figure 7. The end reactions *Q* are:

$$Q = \frac{P(\sec\phi)}{2} \tag{14}$$

Where $\phi = \frac{\theta}{2}$

For $0 < \alpha < \phi$ the transverse moment $M = QR\sin\alpha$ and torsion $T = QR(1-\cos\alpha)$

For $\phi < \alpha < \theta$ the transverse moment $M = QR\sin\alpha - PR\sin(\alpha-\phi)$ and torsion $T = P.R(\cos(\alpha-\phi)-1+\sec\phi.(1-\cos\alpha)/2)$.

The deflection of the ends (at *Q*) relative to the quarter points (at P) can be derived as two components; the first associated with transverse bending alone is $\delta_m = \frac{K.P.R^3}{2EI_t}$ (15a)

Where $K = \frac{(\phi \sec\phi - \sin\phi)}{2}$ (15b)

And I_t is the moment of inertia in the out-of plane direction.

The second component due solely to torsion can be derived as $\delta_t = \frac{k.PR^3}{2GJ}$ (16a)

Where $k = \phi(2.5\sec\phi + 2\cos\phi - 3) - \sin\phi(\sec\phi + 0.5)$ (16b)

In the DR analysis, the total transverse deformations are based only on the twists and torsions related to a reduced torsion constant, $T_{fac} \times GJ$, the torsion factor must therefore be set equal to:

$$T_{fac} = \frac{\delta_t}{\delta_t + \delta_m} = \frac{k}{k + C_1 K} \text{ where } C_1 = \frac{GJ}{EI_t} \quad (17)$$

For the particular case of a circular hollow section with C1=0.8, table 1 gives values of *K*, *k*, and T_{fac} corresponding to values of θ from $\frac{\pi}{2}$ to $\frac{\pi}{64}$.

θ	***K***	***k***	T_{fac}	***Span/Rise***
$\pi/2$	0.20181	0.17777	0.524	2.0
$\pi/4$	0.02118	0.00460	0.214	4.83
$\pi/8$	0.00255	0.00014	0.064	10.05
$\pi/12$	0.00075	18.0×10^{-6}	0.029	15.19
$\pi/16$	0.00032	4.27×10^{-6}	0.016	20.31
$\pi/32$	39.6×10^{-6}	1.33×10^{-6}	0.0042	40.71
$\pi/64$	4.93×10^{-6}	4.15×10^{-6}	0.0011	81.47

Table 1: Values for *K*, *k*, and T_{fac} corresponding to values of θ from $\frac{\pi}{2}$ to $\frac{\pi}{64}$ for a circular hollow section with C1=0.8

The foregoing value of EI_t in equation 17 for bending in the transverse direction (out-of-plane) may be different to the EI value for bending in the radial direction (in-plane), and thus potentially non-circular sections such as rectangular hollow sections could be allowed for. All of the above relates to the particular test cast of transverse loadings at the quarter points of arch beams (with end reaction loads also normal to

the arch), and the values of T_{fac} predicted, although independent of loading magnitude, may not be independent of loading distributions. However, the purpose is to enable the flexibility of arches in the transverse direction to be approximately modeled so the interactions between a flexible membrane surface fields and a supporting arch can be accounted for.

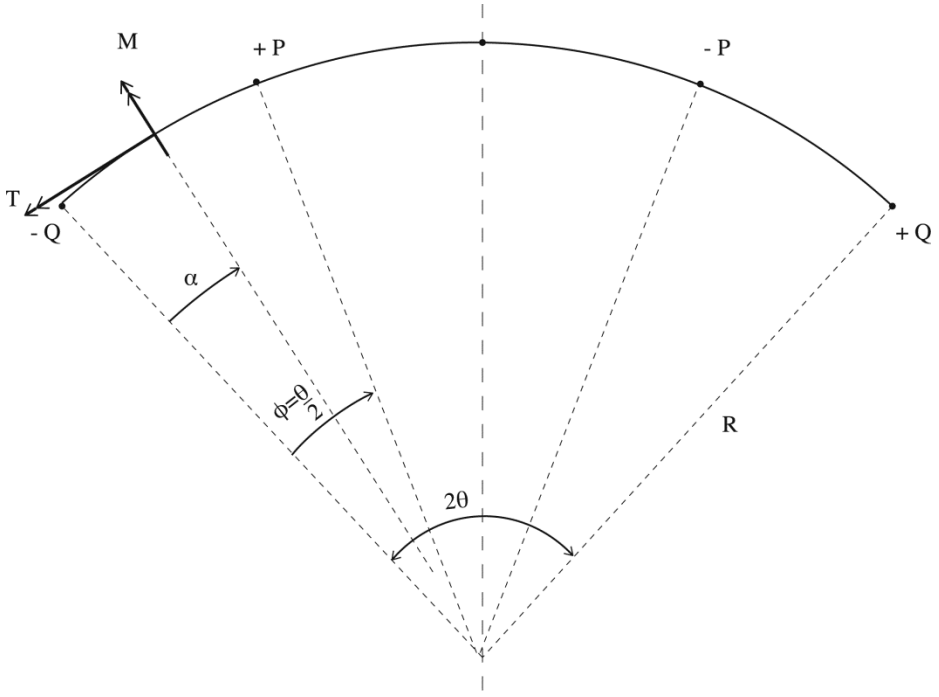

Figure 7: A circular arc beam with radius *R* with equal and opposite transverse loads *P* at the quarter points.

2.3.3. Numerical Stability and Convergence

Numerical stability of the DR process is controlled by fictitious mass components used at each node. These mass components are directly proportional to the stiffness of the elements attached to a node. The elastic axial stiffness of an element is EA/L and the bending stiffness of an arch beam element is $2EI/L^3$. It can be shown that the stiffness of a node due to the coupled torsional and bending effect is $K.(EI/L^3).(R/L)^2$ where R is the in-plane radius of curvature and L is the element length. The value of *K* tends to approach 1, and thus generally $R >> L$. The coupled torsion/bending stiffness and its contribution to the nodal mass component will be very much greater than for ordinary in-plane bending. As a result of these increased mass components, the convergence rate of the DR process is slower for this

type of analysis due to the increased number of iterations. All of the nodal mass components are set automatically within the numerical process, thus the problem of numerical divergence is not an issue. However, a type of quasi-stability can occur when the bending stiffness (in-plane or coupled torsion/transverse bending) are greater than the axial stiffness at any node when the element lengths are very small. To ensure stable convergence in the case of only axial and bending actions: $EA/L > 2EI/L^3$ thus $L^2 > 2I/A = 2r^2$. Hence, for a thin walled tube $L > r$ where r is the mid-thickness tube radius. In the case of coupled torsion/transverse bending it has been found in numerical trials that the least value of element length is approximately $L > 4r + (r.R)^{1/2}/8$.

3. Numerical test cases

The following series of validation tests are for planar arches with circular hollow section of 100m span and varying radii of curvature. All 4 test cases have a ratio $\frac{0.5 \times arclength}{R}$ which correspond with the circular arches with subtended angle between $\pi/4$ and $\pi/16$ studied in section 2.3.2 and presented in Table 1. Two sets of tests are carried out corresponding to two different slenderness ratios, 350 and 500. The circular arches are pin-supported and are loaded perpendicularly out of plane in opposite direction at their quarter points with a point load P. For each test case, deflection at the one-quarter point Δ, the transverse moment at the one-quarter point M_q,the in-plane moment at the quarter point M_o and the torsion at the crown T_c are obtained using the novel torsion/bending formulation for the value of T_{fac} predicted in Table 1, a second value giving a best fit to the theoretical deflection and in the situation where T_{fac} is very small, a value ten times greater. The results are compared with those obtained using the theoretical formulations expressed in equations 15a and 16a, and Numerical Finite Element (FE) predictions. All numerical arches were subdivided in 32 links. The FE models, constructed of beam links with 6 degrees of freedom, were run in a non-linear FE analysis using the commercial software SAP2000 [22]. For all 3 analyses types, the values for deflections, out-of-plane moment, in-plane moment, and the

center point torsion values are tabulated in Table 2 for slenderness ratio 350 and in Table 3 for slenderness ratio 500.

Test Series A: CHS 800mm, t=20mm, span 100m, slenderness ratio L/r_g=350, EA= 10 000MN, EI 800MNm^2,GJ=640MNm^2					
ARC 1A					
$\theta = \pi/4$, R=70.71m,P=100kN					
	T_{fac}	$\Delta = \delta_m + \delta_t$ (m)	M_q (kNm)	M_o (kNm)	T_c (kNm)
Theoretical		0.595	1464		582
Torsion/Bending	0.214	0.530	1455	118 and -161	581
	0.191	0.594	1452	132 and -181	580
FE		0.595	1461	135 and -192	582
ARC 2A					
$\theta = \pi/8$, R=130.66,P=100kN					
	T_{fac}	$\Delta = \delta_m + \delta_t$ (m)	M_q (kNm)	M_o (kNm)	T_c (kNm)
Theoretical		0.379	1299		256
Torsion/Bending	0.064	0.323	1282	185 and -138	256
	0.055	0.378	1275	219 and -156	256
	0.55	0.037	1299	21 and -15	256
FE		0.381	1298	215 and -153	256
ARC 3A					
$\theta = \pi/12$, R=193.19m,P=100kN					
	T_{fac}	$\Delta = \delta_m + \delta_t$ (m)	M_q (kNm)	M_o (kNm)	T_c (kNm)
Theoretical		0.348	1272		167
Torsion/Bending	0.029	0.300	1248	185 and -310	166
	0.025	0.344	1240	212 and -358	165
	0.25	0.034	1272	24 and -29	167
FE		0.349	1270	210 and -352	167
ARC 4A					
$\theta = \pi/16$, R=256.29m,P=100kN					
	T_{fac}	$\Delta = \delta_m + \delta_t$ (m)	M_q (kNm)	M_o (kNm)	T_c (kNm)
Theoretical		0.342	1262		124
Torsion/Bending	0.016	0.295	1222	240 and -430	123
	0.014	0.346	1207	281 and -516	122
	0.14	0.034	1262	33 and -38	124
FE		0.342	1261	275 and -511	124

Table 2: Theoretical, Torsion/Bending and FE deflection and moment results for 4 pin-supported circular arches with slenderness ratio of 350 and of varying heights subjected with opposing out-of plane 100kN point loads at the quarter points.

Test Series B: CHS 570mm, t=15mm, span 100m, slenderness ratio L/r_g=500, EA= 5400MN, EI 220MNm^2,GJ=176MNm^2					
ARC 1B					
$\theta = \pi/4$, R=70.71m,P=50kN					
	T_{fac}	$\Delta = \delta_m + \delta_t$ (m)	M_q (kNm)	M_o (kNm)	T_c (kNm)
Theoretical		1.082	732		291
Torsion/Bending	0.214	0.967	717	107 and -150	289
FE		1.081	732	124 and -165	291
ARC 2B					
$\theta = \pi/8$, R=130.66,P=50kN					
	T_{fac}	$\Delta = \delta_m + \delta_t$ (m)	M_q (kNm)	M_o (kNm)	T_c (kNm)
Theoretical		0.690	650		128
Torsion/Bending	0.064	0.613	620	171 and -135	128
FE		0.700	648	200 and -144	128
ARC 3B					
$\theta = \pi/12$, R=193.19m,P=50kN					
	T_{fac}	$\Delta = \delta_m + \delta_t$ (m)	M_q (kNm)	M_o (kNm)	T_c (kNm)
Theoretical		0.633	636		83
Torsion/Bending	0.029	0.558	596	167 and -369	81
FE		0.633	637	193 and -475	83
ARC 4B					
$\theta = \pi/16$, R=256.29m,P=50kN					
	T_{fac}	$\Delta = \delta_m + \delta_t$ (m)	M_q (kNm)	M_o (kNm)	T_c (kNm)
Theoretical		0.622	631		62
Torsion/Bending	0.016	-	-	-	-
	0.03	0.336	599	180 and -180	64
	0.3	0.029	631	15 and -14	62
FE		0.612	634	201 and -198	62

Table 3: Theoretical, Torsion/Bending and FE deflection and moment results for 4 pin-supported circular arches with slenderness ratio 500 varying heights subjected with opposing out-of plane 50kN point loads at the quarter points.

4. Discussion of results

The out-of-plane static moments and torsions are in all test cases within 1-2% of theoretical predictions, but the transverse deflection, which in the case of coupled curved element and membrane structures will also govern the moments and torsions, is predicted with acceptable accuracy only up to a span/rise ratio of 20, for a slenderness ratio of 350, and 15 for a slenderness ratio of 500 (see Table 2 and 3). These limits would encompass many practical design cases for service loading conditions, but the apparent restriction

on radii of curvature, especially when using torsion factors (T_{fac}) which are preferably automatically set in the analysis program using equations 17 (with equations 15 and 16) must cause difficulties when attempting ultimate load analyses with arches approaching snap-through buckling. As shown in Test Series A and B, the shallower an arch becomes, the smaller is the required value of T_{fac} to give the correct flexibility, but there is a limit to T_{fac} below which numerical convergence cannot be obtained. (ARC 4B).

An additional problem in this context is that the effective coupled torsion/transverse bending stiffness is proportional to $(R/L)^2$ where L is the local element modeling length. An increasing value of *R*, as well as making the arch transversely much stiffer as it flattens, will thus also govern the fictitious mass components which must be used in the DR process to ensure stability and convergence. As snap through buckling is approached the mass factors will need to be greatly increased and simultaneously the value of T_{fac} reduced (with the limit restricted to a least feasible value).

The value of T_{fac} governs the transverse deformations and consequently also the amount of stretch and flattening of the arch crown. These phenomena in turn govern the in-plane moments that are induced (+ve at the ¼ point loading positions and –ve at the crown). These in-plane moments are also related to the amount of twist in the arch, which is greatly increased by the reduced torsion constant ($T_{fac} \times GJ$). In this context the greatest twist at the quarter points in any of the test cases is approximately 10° so it appears that the arch stretching (and the associated crown flattening) is the dominant effect, which is not predicted by the analytical model but confirmed by the non-linear FE model.

5. Application

5.1. Tensile membranes and curved active systems

The simplest and most familiar examples of curved active systems supporting a tensile membrane are slender battens used for pre-stressing umbrellas and igloo camping tents. When an umbrella is opened, a framework of flexible slender steel battens, stretchers and a runner are deployed against a central pole.

This action stresses the loose rayon on nylon cover. In a typical igloo tent, spatially curved elements made of strong yet flexible fibre reinforced plastic or aluminum alloy, fit into the tent pockets of a nylon membrane and are bent into shape and fixed to the ground. In both systems these elements can be very slender because they are stabilized by the pre-stressed membrane. The presented element type makes the form finding and load analysis of tensile membrane and curved active systems at a much larger engineered scale possible. The shape of the solar shade shown in Figure 1b and 8a relies on the boundary element to be sufficiently flexible to be curved into the required form. This element has to resist the forces from bending and twisting into shape while being stiff enough to withstand buckling. In specific design, the element's initial flexibility can be reduced by the membrane's stiffness (as in the case of igloo tents) or alternatively by a cable bracing system that imbues the spatially curved element with additional bending stiffness (and possible shear torsional stiffness).

5.2. Strained grid shells

The numerical form finding of a grid shell can be based on hanging funicular models and its subsequent analysis based on six degrees of freedom models for the various loading combinations. These analyses should clearly account for the initial bending and twisting from straight as an initial strain state (see Figure 8b). The initial shape under the self-weight condition can only be achieved when this strain state is accounted for. For this reason, the presented three degrees of freedom element has clear advantages in a form finding procedure over a hanging model approach as it accurately captures this initial straining.

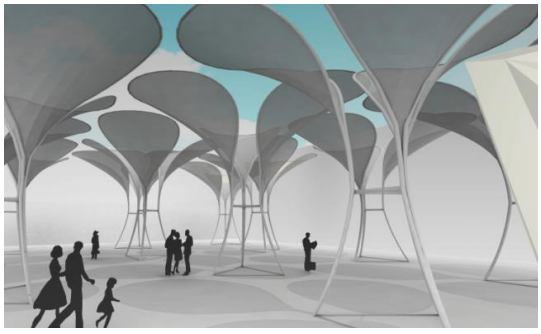

Figure 8: (a) Solar shade that derives its shape from a doubly curved membrane pre-stressed against a three dimensional curved flexible element (PU student project image courtesy S Bagrianski, A Heid, M Krupka) **(b)** The initial shape of a strained grid shell accounts for straining due to bending and torsion. (SG gridshell image courtesy A Kudless, M Cabrinha and D Shook).

6. Conclusion

This paper presents the theory for a novel bending/torsion element that can be incorporated in explicit numerical methods such as DR for the form finding of highly non-linear structures. The element algorithm relies on three translational degrees of freedom only. The coupling of rotational degrees of freedom with axial stiffness and translational degrees of freedom often causes conditioning problems in explicit numerical methods (such as DR) and are thus undesirable in any element formulation. The theory builds on the existing beam element proposed by Adriaenssens and Barnes [20] but extends its scope by accounting for torsion and out-of-plane bending moments. In the DR analysis, the total transverse deformations are based only on the twists and torsions related to a reduced torsion constant. The paper theoretically evaluates this reduction factor or torsional factor for the case of a series of circular arcs with varying subtended angle, but with equal and opposite transverse loads applied at the quarter points. The accuracy of the values for deflection at the one-quarter point, the transverse moment at the one-quarter point, the in-plane moment at the quarter point and the torsion at the crown obtained with the novel element is then validated against the derived theoretical results and numerical non-linear FE results. The results for the test cases have demonstrated the stability and convergence of the process within a DR scheme. The presented element is particularly useful when applied to systems such as grid shells and complex curved and tension active structures.

.

References

[1] F. Otto, Spannweiten, West Berlin: Verlag Ullstein, 1965.

[2] M. Krupka, "Master thesis: Physical and Numerical Form Finding Techniques for Splines Stressed Structures," Princeton University, Princeton, 2012.

[3] A. Day, "An introduction to Dynamic Relaxation," *The Engineer,* vol. 29, pp. 218-221, 1965.

[4] J. Brew and D. Brotton, "Non-linear structural analysis by dynamic relaxation," *International Journal Numerical Methods in Engineering,* vol. 3, no. 1, pp. 463-483, 1971.

[5] P. Cundall, "Explicit finite-difference methods in Geo-mechanics," in *E F Conference on Numerical Methods in Geo-Mechanics,* Blacksburg, 1976.

[6] M. R. Barnes, "Form-Finding and Analysis of tension space structures by Dynamic Relaxation: Ph.D. thesis," City University, London, 1977.

[7] E. Papadrakakis, "Gradient and Relaxation non-linear techniques for the analysis of cable supported structures: Ph.D. thesis," City University, London, 1978.

[8] D. Wakefield, "Dynamic Relaxation Analysis of pre-tensioned networks supported by compression arches: Ph.D. report," City University, London, 1980.

[9] B. Topping, "The application of Dynamic Relaxation to the Design of Modular Space Structures: PhD thesis," The City University, London, 1978.

[10] R. Wood, "A simple technique for controlling element distortion in dynamic relaxation form-finding of tension membranes," *Computers and Structures,* vol. 80, no. 27-30, pp. 2115-2120, 2002.

[11] S. Han and K. Lee, "A study of the stabilizing process of unstable structures by dynamic relaxation method," *Computers and Structures,* vol. 81, no. 17, pp. 1677-1688, 2003.

[12] B. Topping and P. Ivanyi, Computer Aided Design of Cable Membrane Structures, Glasgow: Saxe-Coburg Publications, 2007.

[13] P. Gosling and W. Lewis, "Optimal structural membranes—II. Form-finding of prestressed membranes using a curved quadrilateral finite element for surface definition," *Computers and Structures,* vol. 61, no. 5, pp. 885-895, 1996.

[14] D. Hegyi, I. Sajtos, G. Geizster and K. Hincz, "Eight-node quadrilateral double-curved surface element for membrane analysis," *Computers and Structures,* vol. 84, no. 31-32, pp. 2151-2158,

2006.

[15] J. Rodriguez, G. Rio, J. Cadou and T. J, "Numerical Study of Dynamic Relaxation with kinetic damping applied to inflatable fabric structures with extensions for 3D solid element and non-linear behavior," *Thin-Walled Structres,* vol. 49, no. 11, pp. 1468-1474, 2011.

[16] L. Zhang, B. Maurin and R. Motro, "Form-Finding of Nonregular Tensegrity Systems," *J.Struct.Eng.,* vol. 132, pp. 1435-1441, 2006.

[17] N. Bel Hadj Ali, L. Rhode-Barbarigos and I. Smith, "Analysis of clustered tensegrity structures using a modified dynamic relaxation algorithm," *International Journal of Solids and Structures,* vol. 48, no. 5, pp. 637-647, 2011.

[18] C. Douthe and O. Baverel, "Design of nexorades or reciprocal frame systems with the dynamic relaxation methods," *Computers and Structures,* vol. 87, no. 21-22, pp. 1296-1307, 2009.

[19] K. Hincz, "Nonlinear analysis of cable net structures suspended with arches with block and tackle suspension system, taking into account the friction of the pulleys," *International Journal of Space Structures,* vol. 24, no. 3, pp. 143-152, 2009.

[20] S. Adriaenssens and M. R. Barnes, "Tensegrity spline beam and grid shell structures," *Engineering Structures,* vol. 23, no. 1, pp. 29-36, 2001.

[21] M. Barnes, "Form and stress engineering of tensions structures," *Structural Engineering Review,* vol. 6, no. 3/4, pp. 175-202, 1994.

[22] "SAP2000 Overview," Computers and Structures Inc., [Online]. Available: http://www.csiberkeley.com/sap2000. [Accessed 04 06 2012].

Figures

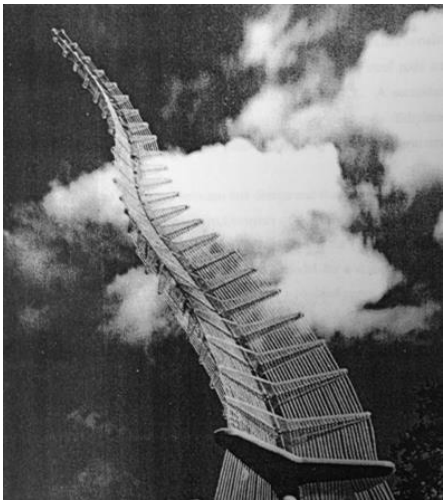

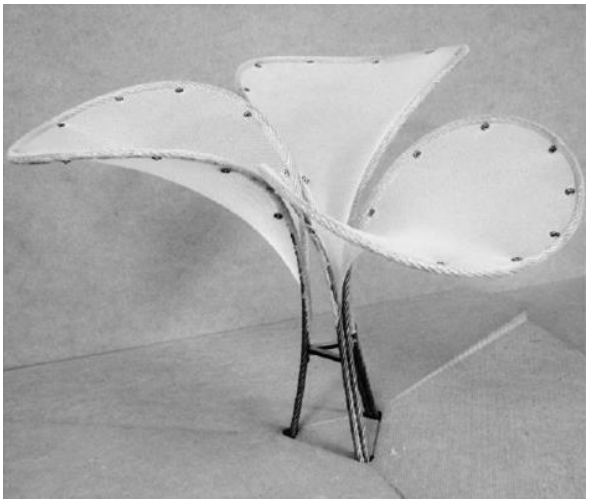

Figure 1 (a) : crane model, a central flexible curve element is shaped by three sets of longitudinal cables **(b)** a twisted and bent element equilibrates with a pre-stressed membrane to form a sun shading structure.(Princeton University student project photo courtesy S Bagrianski, A Heid and M Krupka)

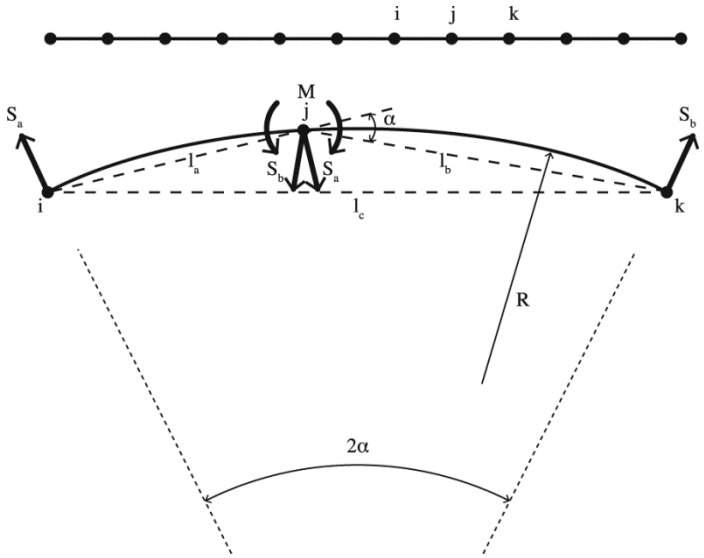

Figure 2: (a) Consecutive nodes along an initially straight tubular beam traverse; (b) Two adjacent deformed segments, a and b, viewed normal to the plane of nodes ijk.

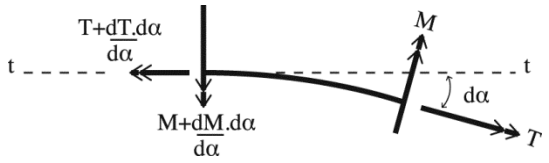

Figure 3: Free body diagram for a small element of a curved element viewed normal to its local plane

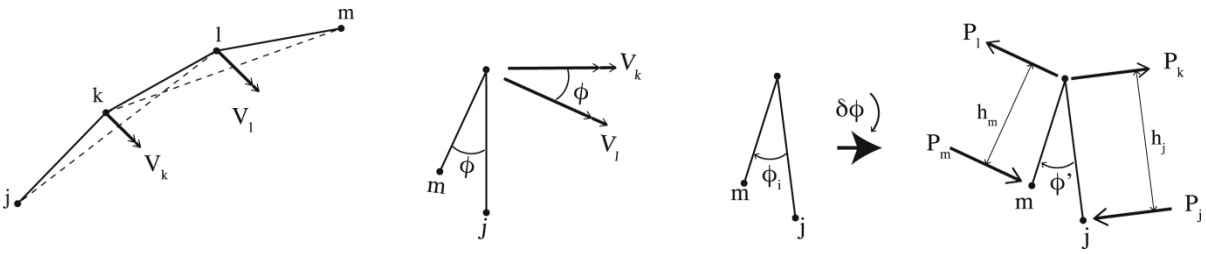

Figure 4 : (a) three consecutive links modeling a curved element going through nodes j,k,l and m and their current normal direction cosine vectors V_k and V_l (side view), **(b,c)** the current twist angle between them ϕ or the initial unstressed state of twist ϕ_i (view in direction parallel with kl), a change in the angle of twist $\delta\phi$ results in a new position **(d)** of the nodes j,k,l and m and sets up restoring forces P_m and P_j at nodes *m* and *j* due to torsion in link *kl* result as well as associated forces P_k and P_l at nodes *k* and *l* to restore the lateral moment equilibrium.

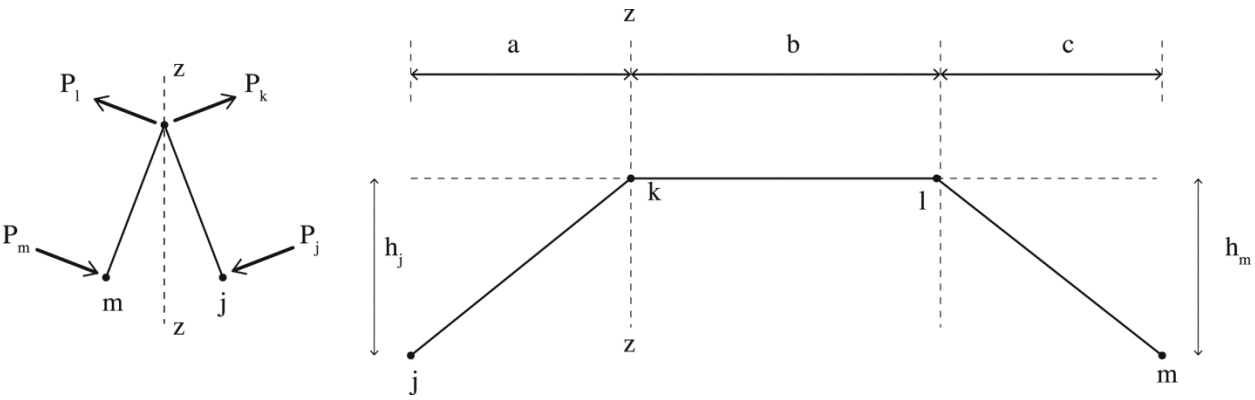

Figure 5: Static equilibrium of the three link unit and side view with dimensions.

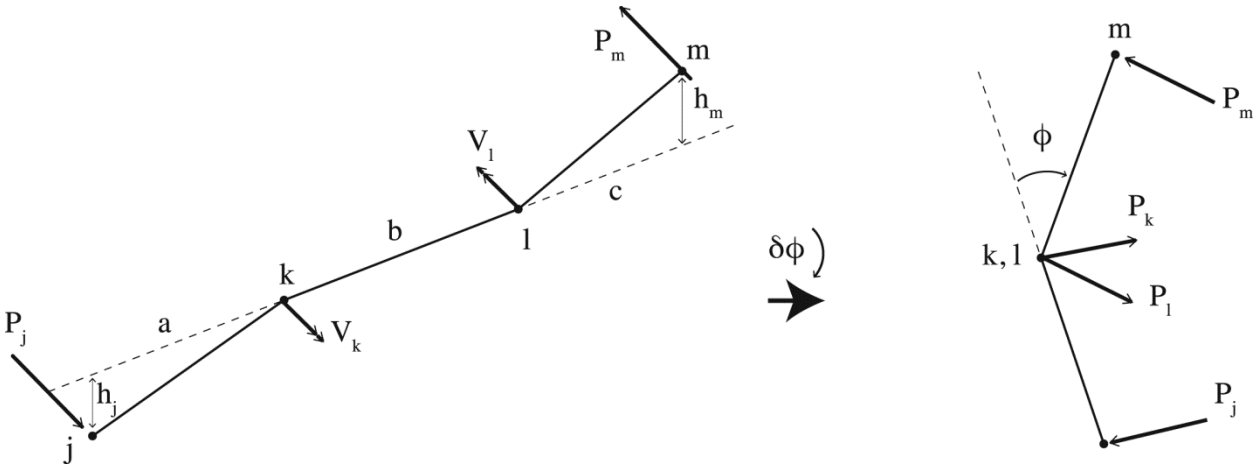

Figure 6: Forces acting on a curved element with inflected sections (**(a)** perspective and **(b)** view parallel with *kl*)

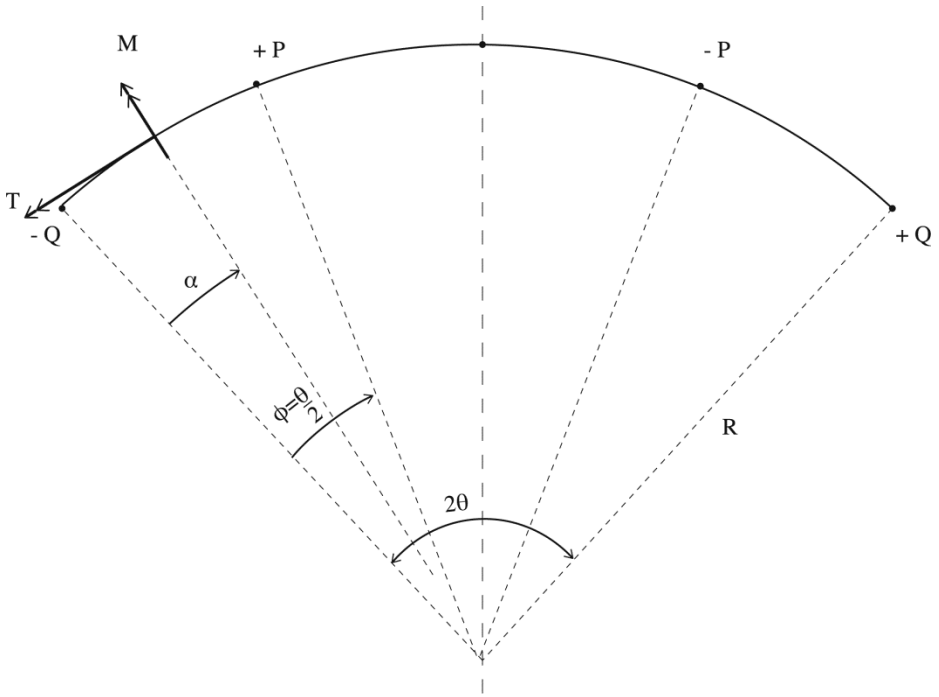

Figure 7: A circular arc beam with radius *R* with equal and opposite transverse loads *P* at the quarter points.

.

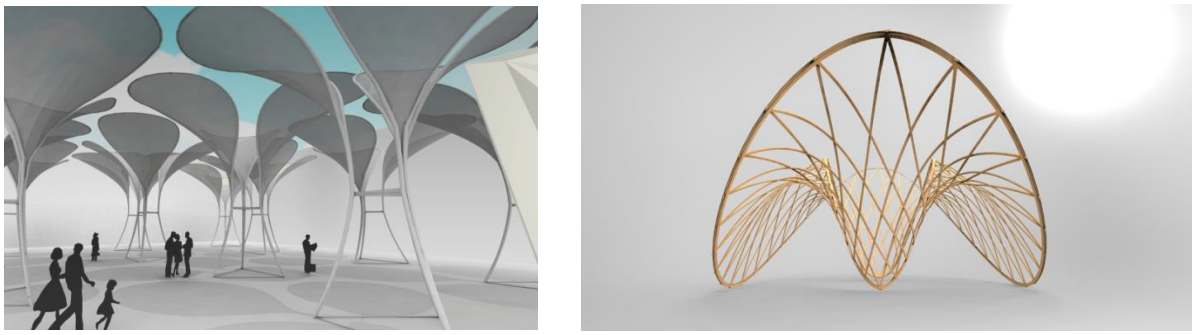

Figure 8: (a) Solar shade that derives its shape from a doubly curved membrane pre-stressed against a three dimensional curved flexible element (PU student project image courtesy S Bagrianski, A Heid, M Krupka) **(b)** The initial shape of a strained grid shell accounts for straining due to bending and torsion. (SG gridshell image courtesy A Kudless, M Cabrinha and D Shook).

Tables

θ	***K***	***k***	T_{fac}	***Span/Rise***
$\pi/2$	0.20181	0.17777	0.524	2.0
$\pi/4$	0.02118	0.00460	0.214	4.83
$\pi/8$	0.00255	0.00014	0.064	10.05
$\pi/12$	0.00075	18.0×10^{-6}	0.029	15.19
$\pi/16$	0.00032	4.27×10^{-6}	0.016	20.31
$\pi/32$	39.6×10^{-6}	1.33×10^{-6}	0.0042	40.71
$\pi/64$	4.93×10^{-6}	4.15×10^{-6}	0.0011	81.47

Table 1: Values for *K*, *k*, and T_{fac} corresponding to values of θ from $\frac{\pi}{2}$ to $\frac{\pi}{64}$ for a circular hollow section with C1=0.8

Test Series A: CHS 800mm, t=20mm, span 100m, slenderness ratio L/r_g=350, EA= 10 000MN, EI 800MNm^2,GJ=640MNm^2					
ARC 1A					
$\theta = \pi/4$, R=70.71m,P=100kN					
	T_{fac}	$\Delta = \delta_m + \delta_t$ (m)	M_q (kNm)	M_o (kNm)	T_c (kNm)
Theoretical		0.595	1464		582
Torsion/Bending	0.214	0.530	1455	118 and -161	581
	0.191	0.594	1452	132 and -181	580
FE		0.595	1461	135 and -192	582
ARC 2A					
$\theta = \pi/8$, R=130.66,P=100kN					
	T_{fac}	$\Delta = \delta_m + \delta_t$ (m)	M_q (kNm)	M_o (kNm)	T_c (kNm)
Theoretical		0.379	1299		256
Torsion/Bending	0.064	0.323	1282	185 and -138	256
	0.055	0.378	1275	219 and -156	256
	0.55	0.037	1299	21 and -15	256
FE		0.381	1298	215 and -153	256
ARC 3A					
$\theta = \pi/12$, R=193.19m,P=100kN					
	T_{fac}	$\Delta = \delta_m + \delta_t$ (m)	M_q (kNm)	M_o (kNm)	T_c (kNm)
Theoretical		0.348	1272		167
Torsion/Bending	0.029	0.300	1248	185 and -310	166
	0.025	0.344	1240	212 and -358	165
	0.25	0.034	1272	24 and -29	167
FE		0.349	1270	210 and -352	167
ARC 4A					
$\theta = \pi/16$, R=256.29m,P=100kN					
	T_{fac}	$\Delta = \delta_m + \delta_t$ (m)	M_q (kNm)	M_o (kNm)	T_c (kNm)
Theoretical		0.342	1262		124
Torsion/Bending	0.016	0.295	1222	240 and -430	123
	0.014	0.346	1207	281 and -516	122
	0.14	0.034	1262	33 and -38	124
FE		0.342	1261	275 and -511	124

Table 2: Theoretical, Torsion/Bending and FE deflection and moment results for 4 pin-supported circular arches with slenderness ratio of 350 and of varying heights subjected with opposing out-of plane 100kN point loads at the quarter points.

Test Series B: CHS 570mm, t=15mm, span 100m, slenderness ratio L/r_g=500, EA= 5400MN, EI 220MNm^2,GJ=176MNm^2					
ARC 1B					
$\theta = \pi/4$, R=70.71m,P=50kN					
	T_{fac}	$\Delta = \delta_m + \delta_t$ (m)	M_q (kNm)	M_o (kNm)	T_c (kNm)
Theoretical		1.082	732		291
Torsion/Bending	0.214	0.967	717	107 and -150	289
FE		1.081	732	124 and -165	291
ARC 2B					
$\theta = \pi/8$, R=130.66,P=50kN					
	T_{fac}	$\Delta = \delta_m + \delta_t$ (m)	M_q (kNm)	M_o (kNm)	T_c (kNm)
Theoretical		0.690	650		128
Torsion/Bending	0.064	0.613	620	171 and -135	128
FE		0.700	648	200 and -144	128
ARC 3B					
$\theta = \pi/12$, R=193.19m,P=50kN					
	T_{fac}	$\Delta = \delta_m + \delta_t$ (m)	M_q (kNm)	M_o (kNm)	T_c (kNm)
Theoretical		0.633	636		83
Torsion/Bending	0.029	0.558	596	167 and -369	81
FE		0.633	637	193 and -475	83
ARC 4B					
$\theta = \pi/16$, R=256.29m,P=50kN					
	T_{fac}	$\Delta = \delta_m + \delta_t$ (m)	M_q (kNm)	M_o (kNm)	T_c (kNm)
Theoretical		0.622	631		62
Torsion/Bending	0.016	-	-	-	-
	0.03	0.336	599	180 and -180	64
	0.3	0.029	631	15 and -14	62
FE		0.612	634	201 and -198	62

Table 3: Theoretical, Torsion/Bending and FE deflection and moment results for 4 pin-supported circular arches with slenderness ratio 500 varying heights subjected with opposing out-of plane 50kN point loads at the quarter points.